Early afterdepolarisations and ventricular arrhythmias in cardiac tissue: A computational study

Simon Scarle* and Richard .H. Clayton[¶]

Department of Computer Science, University of Sheffield, Regent Court, 211 Portobello Street, Sheffield, S1 4DP, UK.

[¶]*Corresponding author*
Postal address: Department of Computer Science, University of Sheffield, Regent Court, 211 Portobello Street, Sheffield, S1 4DP, UK.
Telephone: (+44) 114 222 1845
Fax: (+44) 114 222 1810
email: r.h.clayton@sheffield.ac.uk

*Current Address: Rare Ltd., Manor Park, Twycross, Warwickshire., CV9 3QN, UK.

keywords: heart, re-entry, fibrillation, excitable media, early afterdepolarisations

Submitted to Medical and Biological Engineering and Computing, and accepted pending minor revision 1 September 2008

The final typeset version of this manuscript will be available at http://www.springerlink.com/content/0140-0118

Abstract

Afterdepolarisations are associated with arrhythmias in the heart, but are difficult to study experimentally. In this study we used a simplified computational model of 1D and 2D cardiac ventricular tissue, where we could control the size of the region generating afterdepolarisations, as well as the properties of the afterdepolarisation waveform. Provided the size of the afterdepolarisation region was greater than around 1 mm, propagating extrasystoles were produced in both 1D and 2D. The number of extrasystoles produced depended on the amplitude, period, and duration of the oscillatory EAD waveform. In 2D, re-entry was also initiated for specific combinations of EAD amplitude, period, and duration, with the afterdepolarisation region acting as a common pathway. The main finding from this modelling study is therefore that afterdepolarisations can act as potent sources of propagating extrasystoles, as well as a source of re-entrant activation.

Introduction

Computational models of cardiac cells and tissue are becoming an important research tool for studying the mechanisms that initiate and sustain arrhythmias in the heart. Afterdepolarisations are depolarisation of the cardiac membrane potential occurring either during or soon after repolarisation. Depolarisation occurring during repolarisation is classified as an early afterdepolarisation (EAD), whilst depolarisation occurring after repolarisation is complete is classified as a delayed afterdepolarisation (DAD). Afterdepolarisations can provide both the trigger and the substrate for initiating cardiac arrhythmias [1] by generating closely coupled extrasystoles and by acting as regions of heterogeneous repolarisation. If an afterdepolarisation is of sufficient magnitude that it brings the membrane potential of neighbouring tissue to threshold, an extrasystole can result. Experimental studies have shown that EADs can initiate propagating extrasystoles, and that these in turn can initiate arrhythmias in both atria and ventricles [2, 3].

The mechanisms of afterdepolarisations have been investigated in some detail at the cellular level, and these studies show that a switch in the balance of current flow across the cell membrane from outward to inward during or following repolarisation can produce an afterdepolarisation. Computational studies have shown that reactivation of the inward Ca^{2+} current associated with either a reduction in outward K^+ currents during repolarisation, or reversal of the Na^+/Ca^{2+} exchanger current following spontaneous Ca^{2+} release from the sarcoplasmic reticulum are both plausible explanations [4]. The role of reduced K^+ current flow is consistent with the increased incidence of afterdepolarisations and arrhythmias associated with the long

QT syndromes [3]. The role of intracellular Ca^{2+} overload and spontaneous release is supported by experimental studies showing that synchronised release of [Ca^{2+}] is associated with EAD activity and travelling waves of Ca^{2+} release are associated with of DAD activity [1, 5].

Computational studies have concentrated on either the cellular mechanisms underlying EADs [4], or on the role of EADs in destabilising and re-initiating re-entry [6]. However, although EADs are widely believed to initiate arrhythmias in cardiac ventricular tissue, the interaction of EAD regions with normal tissue to initiate propagating extrasystoles and re-entry remains incompletely understood. This is in part because EADs are difficult to record from tissue [3]. Experimental studies have shown that afterdepolarisations can be suppressed by the electrotonic effect of normal tissue [7], and coupling between regions of tissue generating EADs and surrounding tissue is recognised as important for the generation of a propagating extrasystole [8].

The aim of this work was therefore to study how the size of the region of tissue generating an EAD and the EAD waveform characteristics influence the initiation of arrhythmias. Experimental studies show a wide variety of EAD configurations ranging from a single hump in phase 2 or phase 3 of the action potential to several oscillations of membrane potential [3, 9, 10]. By using a computational model we were able to tightly control not only the location and size of EAD capable regions, but also the EAD waveform characteristics, neither of which can be easily achieved in an experimental model.

Methods

Cell and Tissue Model

Cardiac tissue can be modelled as an electrically excitable medium which supports travelling waves of electrical activation. This system can be described by a non-linear reaction diffusion equation [11]

$$C_m \frac{\partial V_m}{\partial t} = \nabla \cdot \mathbf{D} \nabla V_m - I_{ion} \quad (1)$$

The left hand side of Equation 1 gives current flow due to the capacitance of the cell membrane, whilst the right hand side gives current flow due to gradients in trans-membrane potential (diffusive term = $\nabla \cdot \mathbf{D} \nabla V_m$), and ion channels, pumps and transporters in the cell membrane (reaction term = I_{ion}). For isotropic diffusion of voltage, the diffusion tensor $\mathbf{D}$ is a diffusion coefficient D with units of mm^2ms^{-1}, V_m is voltage across the cell membrane, C_m is membrane capacitance per unit membrane area, and I_{ion} is membrane current flow per unit area.

It has been well established that accumulation and spontaneous release of intracellular Ca^{2+} can produce abnormal electrical activity such as EADs or DADs [2], because intracellular [Ca^{2+}] affects a number of different membrane currents: in particular the Na^+-Ca^{2+} exchanger current I_{NaCa}, the L-type Ca^{2+} channel current $I_{Ca,L}$ and the Ca^{2+} activated non selective current I_{nsCa}. Second generation ionic models of cardiac cells include detailed descriptions of storage and release of intracellular Ca^{2+} [12], and this type of detailed and computationally intensive model has been used to investigate EAD and DAD mechanisms by inducing intracellular Ca^{2+} accumulation

and overload [13], or by partial block of ion channels involved in repolarisation [14]. There is a trend towards models of cardiac myocytes that also include local control of Ca^{2+} release [15], but even when simplified [16] these models are computationally intensive to solve. Models with a less detailed representation of Ca^{2+} handling can show EAD like behaviour when ion channel conductances are modified, however EADs are obtained for only very small ranges of channel conductance [17], and it is difficult to establish whether this is a physiologically plausible mechanism or a merely an instability in the computational model.

The focus of the present study was to investigate how EADs can produce arrhythmias in cardiac tissue. Instead of using a biophysically detailed model to generate EAD behaviour, we chose to modify a simplified phenomenological model of the cardiac action potential. By taking this approach, we could control the shape and duration of the EAD waveform without making any assumptions about the underlying physiology.

The 4 variable simplified ionic model (4VSIM) has been developed for cardiac tissue simulations [18, 19]. The model equations and parameter values used in this study are given in the Appendix. In this simplified model I_{ion} is expressed as the sum of three current densities J_{fi}, J_{si} and J_{so}. J_{fi} and J_{si} are fast and slow inward currents corresponding broadly to the inward currents carried by Na^+ and Ca^{2+} ions in real cardiac cells. J_{so} is a slow outward current broadly corresponding to outward currents carried mostly by K^+ ions in real cardiac cells. These current densities do not actually represent measured currents, but only their activation, inactivation and reactivation dynamics. It is these dynamics which are needed to qualitatively reproduce the action

potential shape and restitution properties of the cardiac cell membrane. The membrane potential V_m is rescaled to be a dimensionless activation, u, that varies between 0 (-85 mV) and 1 (+15 mV). The currents J_x are governed by three gating variables v, w and s, each of which varies between 0 and 1. These variables have time and voltage dependent characteristics described by the ordinary differential equations given in the Appendix and illustrated in Figure 1a. J_{fi} depolarises the membrane to create the action potential upstroke. It is activated when u crosses a threshold u_c, and is inactivated by v. J_{si} is controlled by w and s, which in turn depend on u. J_{so} depends on u and acts to repolarise the membrane.

All simulations for this study were carried out by solving Equation 1 using an explicit finite difference numeric integration. We set C_m to 1 μF cm^{-2}, D to 0.0005 cm^2 ms^{-1}, and employed no-flux boundary conditions. In simulations of isotropic 1D and 2D tissue we used a space step of 0.02 cm and a time step of 0.01 ms, which gave a plane wave conduction velocity of 0.35 ms^{-1}. All computations used double precision arithmetic. When the time step was increased to 0.04 ms and the space step increased to 0.25 mm plane wave conduction velocity fell to 0.33 ms^{-1}, indicating stability of the numerical scheme for our chosen combination of time and space step. At the start of each simulation the variables u, v, w and s were set to their resting values of 0, 1, 1, and 0, and propagating action potentials were initiated by applying a current stimulus for 1 ms to two grid points at one end of the 1D fibre or to two columns of grid points at one edge of the 2D sheet.

We used a parameter set (F.H. Fenton and E.M. Cherry, personal communication, and provided in the Appendix) for the 4VSIM equations that reproduced the action

potential shape and APD restitution of canine epicardial cells (Figure 1a). This model was adapted to reproduce EAD like behaviour by switching on a sinusoidal oscillation in membrane potential u (and u only) for a fixed duration during repolarisation as described below. The other variables v, w, and s in the 4VSIM model were not changed, and were only affected indirectly.

EAD simulation

In our tissue model, normal regions were governed purely by 4VSIM kinetics, whilst EAD capable regions had three additional states, described as follows:

State One EAD capable regions behaved as normal 4VSIM tissue until all the following conditions were met, corresponding with repolarisation to about -15 mV:

$$0.5 < s < 0.6, \quad \frac{ds}{dt} < 0, \ \frac{du}{dt} < 0 \tag{2}$$

upon which they became State Two.

State Two In this state, EAD capable regions adopted purely oscillatory u behaviour using the equation 3 to evaluate u:

$$\frac{du}{dt} = -\frac{2\pi A}{P}\cos\left(\frac{2\pi(t-T)}{P}\right) \tag{3}$$

where A is the EAD amplitude, P the EAD period, and T the time at which oscillations start. After the EAD had lasted for a specified EAD duration, State Two regions became State Three.

State Three Following an EAD, these regions returned to normal 4VSIM behaviour for the rest of the simulation.

This model produced EAD behaviour as shown in Figure 1b, which shows the transition to EAD behaviour during repolarisation. The EAD period (60 ms in this example) and EAD duration (390 ms in this example) are labelled in Figure 1b, and the EAD amplitude is the amplitude of the sinusoidal oscillations (0.2 in this example).

Results

1D fibre – central EAD capable region

Previous computational studies have indicated that the number of cells producing abnormal electrical activity is critical in determining whether a propagating extrasystole will be generated [20]. This idea is similar to the concept of liminal length in neuronal propagation. In this part of the study we therefore examined the role of EAD region size, EAD amplitude, EAD period, and EAD duration on the number of antegrade and retrograde extrasystoles produced in a 1D fibre. These simulations used a 4 cm long 1D fibre, where the central region was EAD capable. The size of the EAD capable region was set to 5, 15, and 25 mm, the EAD amplitude was set to 0.2, 0.4, and 0.6 (corresponding to 20, 40, and 60 mV), EAD period was set to 20,

40, 60, 80, and 100 ms, and EAD duration set to 400 ms. In a subsequent set of simulations the effect of EAD duration was set to 100, 200, 300, 400, 500, and 600 ms, with EAD amplitude and EAD region size fixed to 0.4 and 15 mm respectively.

The overall results are presented in Table 1 and Table 2, where the responses are labelled as 0 for simulations that produced no extrasystoles, A for an antegrade extrasystole, and R for a retrograde extrasystole. We have used space-time plots (explained in Figure 2) to illustrate the main findings from this part of the study in Figures 3 and 4.

Figure 3 shows the effect of changing the size of the EAD capable region and the EAD amplitude in a 1-D fibre. The top row of space-time plots shows simulations with an EAD region size of 5 mm, and an EAD amplitude of 0.2 (left), 0.4 (middle), and 0.6 (right). The middle and lower rows show simulations with EAD region size of 15 mm (middle) and 25 mm (bottom). The broadly similar space-time plots in each row show that the size of the EAD region had only a modest effect on the number of propagating extrasystoles. Although the EAD waveform was attenuated by electrotonic effects at the edges of the EAD region, this effect was not sufficient to suppress the EAD completely even for the smallest 5 mm region. Additional simulations with an EAD period of 60 ms established that the minimum size of the EAD region that produced a propagating extrasystole was 1.4 mm (7 grid points) for an EAD amplitude of 0.4, and 0.8 mm (4 grid points) for an EAD amplitude of 0.6.

Changing EAD amplitude resulted in changes to the pattern of extrasystoles, and this effect is illustrated by comparing the columns of Figure 3. At the lowest amplitude

(left hand column), the EAD oscillation was not large enough to elicit a propagating action potential in the surrounding normal tissue. For larger EAD region sizes, the amplitude 0.4 EAD elicited a single antegrade and a single retrograde extrasystole. The amplitude 0.6 EAD elicited these extrasystoles earlier, and so the surrounding normal tissue had recovered enough for a second pair of extrasystoles to be elicited. In general, larger EAD amplitudes produced more extrasystoles, and this can be seen clearly in Table 1.

Figure 4 shows the effect of EAD duration and EAD period for a 1-D fibre with EAD region size of 15 mm and EAD amplitude of 0.4. Each row shows space-time plots for EAD durations of 100, 200, 300, 400, 500, and 600 ms, from left to right. EAD period was 40 ms (top row), 60 ms (middle row), and 80 ms (bottom row). Comparison of the columns in Figure 4 and Table 2 shows that EAD duration had a strong influence on the number of propagating extrasystoles, but comparison of rows shows that EAD period had a modest influence on propagating extrasystoles. A short EAD did not last long enough for the surrounding tissue to recover, and so produced no propagating extrasystole. As EAD duration increased, the surrounding tissue recovered, and was able to support one or more propagating extrasystoles. Changing EAD period influenced the timing of peaks in the EAD waveform, and so the determined whether extrasystoles were elicited at the end of the EAD.

2D sheet – central EAD capable region

2D simulations were carried out with a geometry which extended our previous 1D simulations, so that the size of the EAD region became the diameter of a circular EAD capable zone located in the centre of a 6 x 6 cm tissue sheet. For these

simulations we set EAD amplitude to a single value of 0.4. We set the radius of the EAD capable region to 10, 20, and 25 mm, EAD period to 20, 40, 60, 80, and 100 ms, and EAD duration to 200, 400, and 600 ms.

Figure 5 shows examples of the different types of behaviour produced in the 2D simulations; with an EAD radius of 20 mm, EAD duration of 400 ms, and EAD period varying from 40 ms (Figure 5a) to 100 ms (Figure 5d). Movie files for these simulations are provided as supplementary data. Figure 5(a) shows that with an EAD period of 40 ms, the EAD region acted as a focal source for two propagating extrasystoles. In the first snapshot (370 ms), the arrows indicate the direction of propagation of the preceding beat, and the dotted line indicates the boundary of the EAD capable region. The two stars indicate where the EAD capable region initiated activation in the surrounding normal tissue, which can be seen propagating in retrograde and antegrade directions in the next snapshot (400 ms). At 425 ms (not shown), a further activation was initiated at the right hand edge of the EAD capable region, and this then collided with the first activation to result in a single extrasystole. Another pair of activations were initiated simultaneously at 615 ms, resulting in the pattern shown at 650 ms. The 2D behaviour was therefore different from the corresponding 1D behaviour shown in Figure 4, where two retrograde and one antegrade extrasystoles were produced, because the activations propagated around the edge of the EAD capable region and collided to produce a single extrasystole.

Changing EAD period modulated the timing of activations, and influenced whether one or two activations were produced. Figure 5(b) shows that for an EAD period of 60 ms, only one activation was produced at 650 ms, and since it did not collide with a

retrograde activation it was able to re-enter the EAD capable zone resulting in sustained re-entry. Figure 5(c) shows that similar behaviour was also observed when the EAD period was 80 ms, but in this case the re-entrant wave was subsequently blocked before it could exit the EAD capable region. In Figure 5(d), increasing the EAD period to 100 ms resulted in a single extrasystole, which was blocked from re-entering the EAD capable region.

The key difference between the 1D and 2D simulations was therefore that breakthrough of activation from the EAD region into surrounding tissue could occur around the circumference of the circular EAD capable region. These breakthrough activations could collide, or re-enter the EAD capable region. Thus by moving our model system into 2-D, we gained a greater degree of freedom by which our EAD capable cells can produce arrhythmias.

The exact pattern of behaviour depended on the timing and location of breakthrough from the EAD capable region, which in turn depended on the period and duration of the EAD. Table 3 shows the outcome of the all 2D simulations, and shows that a longer EAD duration of 400 or 600 ms and an EAD period of less than 100 ms favoured re-entry. As in 1D, the size of the EAD region had only a small effect on behaviour.

Discussion

In this study we have used a simplified model of EAD activity in 1D and 2D cardiac tissue to speculate about how EADs can act as a source and trigger for ventricular

arrhythmias in the heart. In both 1D and 2D simulations we found that the size of the EAD capable region did not greatly affect the patterns of activity produced, providing that the EAD capable region was larger than around 1 mm. The EAD amplitude, EAD period, and EAD duration all had an effect on the number of extrasystoles produced by the simulated EAD behaviour. Increased EAD amplitude and increased EAD duration resulted in more propagating extrasystoles, whereas EAD period modulated the number of antegrade and retrograde extrasystoles in 1D, and the incidence of re-entry in 2D.

EADs as a trigger for arrhythmias

Based on these findings, we propose that a region of EAD capable tissue can act to initiate re-entrant ventricular arrhythmias in three ways. First, we have shown in the present study that if subsequent EAD activity is suppressed by short cycle lengths (as in our model), re-entry may occur with a common pathway through the EAD capable region, providing the EAD capable region is large enough. Second, we have shown that an EAD capable region can act as a focal source of closely coupled extrasystoles. There is good theoretical and experimental evidence to show that a critically timed extrasystole can initiate re-entry [22], but in the present study we did not address how the extrasystoles produced by EAD activity could initiate re-entry by this mechanism. Third, the APD restitution curve determines the dynamical behaviour of tissue, and a sequence of closely coupled extrasystoles could produce re-entry through instability resulting from steepness of the APD restitution curve [23]. Again we did not address this question explicitly in the present study, but evidence from computational and experimental studies shows that re-entry may be produced in this way [24].

Influence of EAD region size and waveform characteristics

In this study we assumed that some regions of tissue were EAD capable whereas some were not, and this assumption was based on experimental data showing focal initiation of extrasystoles [2], as well as evidence for heterogeneity of Ca^{2+} handling in the ventricles [25].

Although we found that the size of the EAD capable region did not have a great influence on the pattern of activation produced as long as it was greater than a critical value, we only considered circular shaped regions in our 2D simulations, with a sharp division between EAD capable and normal regions. In real cardiac tissue it is possible that there are gradients in the parameters favouring EAD activity, resulting in diffuse EAD capable regions.

We found that propagating extrasystoles were only produced in 1D if the size of the EAD capable region was greater than around 1 mm. This value is close to estimates of the longitudinal space constant ($\lambda_m \approx 1$ mm), but lower than estimates of liminal length ($0.1\ \lambda_m - 0.2\ \lambda_m$) obtained from Purkinje fibres [21]. However, the minimum size of an EAD capable region will depend on cell to cell coupling, and would be smaller with a lower diffusion coefficient.

We chose to simulate the EAD waveform using a sinusoid, since this is a reasonable approximation to the EAD waveforms documented in the literature [3, 9, 10]. EAD

amplitude and duration influenced the number of extrasystoles produced, whereas the influence of EAD period was more subtle because the timing of an extrasystole depended on the upstroke of the EAD, and the recovery or adjacent normal tissue. The interaction of these two properties determined whether activation was initiated in recovered normal tissue, and this effect can be clearly seen in Figure 4 and Figure 5. In both models and real cardiac tissue, electrotonic effects act to smooth the upstroke of an action potential, and so we might have expected the EAD waveforms with a longer period (and hence a smaller dV/dt) to be less able to initiate a propagating extrasystole. This was not the case for the range of EAD period included in the study, although additional simulations established that for an EAD duration of 400 ms and EAD amplitude of 0.4, no propagating extrasystoles were produced for EAD period greater than 280 ms.

Further work

This study raises three specific questions that could be addressed by future studies.

First, we focussed on how EADs can produce propagating extrasystoles in a simplified 1D and 2D model of cardiac tissue. Real cardiac tissue is anisotropic, and has a complex 3D shape. The present study has shown that the interaction of EAD capable regions with normal tissue can produce a rich variety of behaviours in 2D. In 3D tissue it is likely that these behaviours will be further modulated by anisotropy. As noted above, we did not investigate how extrasystoles produced by EADs could subsequently trigger re-entry, and it would be valuable to explore this triggering effect in 3D.

Second, we used a simplified model of the cardiac action potential, which enabled us to concentrate on the tissue effects of EADs. The underlying cellular mechanisms that produce EADs are clearly important, and further work with biophysically detailed cell models [4, 29] would enable the parameters that are important for determining EAD waveform shape to be identified. Detailed cell models combined with anatomically detailed models of 3D ventricular anatomy [30, 31] also have the potential to identify new therapeutic targets to suppress EAD activity. The use of anatomically detailed models of tissue would also enable tissue mechanics to be included [32]. Electrical recovery is associated with tension generation in cardiac tissue as well as EAD activity. The effect of stretch on ion channel conductivity results in coupling of mechanical to electrical activity [33], and so it is possible that local tension influences both EAD activity and the ability of an EAD to initiate a propagating extrasystole.

Third, although most experimental evidence supports the idea that ventricular fibrillation is sustained by re-entry [26], focal mechanisms may play a role [27, 28]. It is possible that EAD activity may underlie sustained arrhythmias; this question was not addressed in the present study because EAD behaviour was ‘switched off’ following the first EAD. However, the findings of recent computational studies indicate that EADs are capable of destabilising re-entrant arrhythmias [29], and this idea has important implications for our understanding of ventricular fibrillation mechanisms.

Conclusion

The main finding from this modelling study is that EAD capable regions of cardiac tissue can act as potent sources of propagating extrasystoles, as well as a source of re-entrant activation. The amplitude and duration of the EAD waveform determined the number of extrasystoles produced, and the period of oscillations in the EAD waveform influenced their timing. In 2D, the EAD period determined the likelihood of re-entry through the EAD capable region.

Acknowledgements

We would like to thank the British Heart Foundation for funding this work through the award of Project Grant PG/03/102/1582. We would also like to thank both the Integrative Biology eScience project (EPSRC GR/S72023/01) and the White Rose Grid (www.wrgrid.org.uk) for making computer resources available for this work. We are especially grateful to Flavio Fenton and Elizabeth Cherry from Cornell University for providing parameter sets and source code for the 4VSIM model.

References

[1] Volders PGA, Vos MA, Szabo B, et al. (2000) Progress in the understanding of cardiac early afterdepolarizations and torsades de pointes: time to revise current concepts. Cardiovascular Research 46:376-392.

[2] Choi B-R, Burton F, Salama G (2002) Cytosolic Ca2+ triggers early afterdepolarizations and Torsade de Pointes in rabbit hearts with type 2 long QT syndrome. Journal of Physiology (London) 543:615-631.

[3] Yan G-X, Y. W, T. L, et al. (2001) Phase 2 early afterdepolarization as a trigger of polymorphic ventricular tachycardia in acquired long-QT syndrome: Direct evidence from intracellular recordings in the intact left ventricular wall. Circulation 103:2851-2856.

[4] Viswanathan PC, Rudy Y (1999) Pause induced early afterdepolarizations in the Long-QT syndrome: A simulation study. Cardiovascular Research 42:530-542.

[5] ter Keurs HEDJ, Boyden PA (2007) Calcium and arrhythmogenesis. Physiological Reviews 87:457-506.
[6] Huffaker R, Lamp S, Weiss J, et al. (2004) Intracellular calcium cycling, early afterdepolarizations, and reentry in simulated long QT syndrome. Heart Rhythm 1:441-8.
[7] Huelsing DJ, Spitzer KW, Pollard AE (2000) Electrotonic suppression of early afterdepolarizations in isolated rabbit Purkinje myocytes. American Journal of Physiology (Heart and Circulatory Physiology) 279:H250-259.
[8] Schafferhofer-Steltzer I, Hofer E, Huelsing DJ, et al. (2005) Contributions of Purkinje-Myocardial coupling to suppression and facilitation of early afterdepolarization-induced triggered activity. IEEE Transactions on Biomedical Engineering 52:1522-1531.
[9] Gilmour JRF, Moise NS (1995) Triggered activity as a mechanism for inherited ventricular arrhythmias in German shepherd dogs. Journal of the American College of Cardiology 27:1526-1533.
[10] Sosunov EA, Anhuyovsky EP, Shivilkin A, et al. (1999) Abnormal cardiac repolarization and impulse initiation in German shepherd dogs with inherited ventricular arrhythmias and sudden death. Cardiovascular Research 42:65-79.
[11] Clayton RH (2001) Computational models of normal and abnormal action potential propagation in cardiac tissue: Linking experimental and clinical cardiology. Physiological Measurement 22:R15-R34.
[12] Rudy Y (2006) Computational biology in the study of cardiac ion channels and cell electrophysiology. Quarterly Reviews of Biophysics 39:57-116.
[13] Luo CH, Rudy Y (1994) A Dynamic-Model of the Cardiac Ventricular Action-Potential .2. Afterdepolarizations, Triggered Activity, and Potentiation. Circulation Research 74:1097-1113.
[14] Zeng JL, Rudy Y (1995) Early Afterdepolarizations in Cardiac Myocytes - Mechanism and Rate Dependence. Biophysical Journal 68:949-964.
[15] Greenstein J, Winslow R (2002) An Integrative Model of the Cardiac Ventricular Myocyte Incorporating Local Control of Ca2+ Release. Biophysical Journal 83:2918-2945.
[16] Hinch R, Greenstein J, Tanskanen A, et al. (2004) A Simplified Local Control Model of Calcium-Induced Calcium Release in Cardiac Ventricular Myocytes. Biophysical Journal 87:3723-3736.
[17] Clayton RH, Holden AV, Tong WC (2003) Can endogenous, noise-triggered early afterdepolarisations initiate re-entry in a modified Luo-Rudy virtual tissue? International Journal of Bifurcation and Chaos 13:3835-3843.
[18] Fenton FH, Cherry EM, Hastings HM, et al. (2002) Multiple mechanisms of spiral wave breakup in a model of cardiac electrical activity. Chaos 12:852-892.
[19] Cherry EM, Ehrlich JR, Nattel S, et al. (2007) Pulmonary vein re-entry - Properties and size matter: Insights from a computational analysis. Heart Rhythm 4:1553-1562.
[20] Henriquez AP, Vogel R, Muller-Borer BJ, et al. (2001) Influence of dynamic gap junction resistance on impulse generation in ventricular myocardium: A computer simulation study. Biophysical Journal 81:2112-2121.
[21] Fozzard HA, Schoenberg M (1972) Strength-duration curves in cardiac Purkinje fibres: effects of liminal length and charge distribution. Journal of Physiology 226:593-618.

[22] Winfree AT (1989) Electrical instability in cardiac muscle. Journal of Theoretical Biology 138:353-405.
[23] Karma A (1993) Spiral breakup in model equations of action potential propagation in cardiac tissue. Physical Review Letters 71:1103-1107.
[24] Swissa M, Qu ZL, Ohara T, et al. (2002) Action potential duration restitution and ventricular fibrillation due to rapid focal excitation. American Journal of Physiology (Heart and Circulatory Physiology) 282:H1915-H1923.
[25] Katra R, Pruvot E, Laurita KR (2004) Intracellular calcium handling heterogeneities in intact guinea pig hearts. American Journal of Physiology (Heart and Circulatory Physiology) 286:H648-H656.
[26] Gray RA, Pertsov AM, Jalife J (1998) Spatial and temporal organization during cardiac fibrillation. Nature 392:75-78.
[27] Pogwizd SM, Corr PB (1990) Mechanisms underlying the development of ventricular fibrillation during early myocardial ischaemia. Circulation Research 66:672-695.
[28] Pogwizd SM, Corr PB (1992) The contribution of nonreentrant mechanisms to malignant ventricular arrhythmias. Basic Research in Cardiology 87:115-129.
[29] Huffaker R, Weiss JN, Kogan B (2007) Effects of early afterdepolarizations on re-entry in cardiac tissue: a simulation study. American Journal of Physiology (Heart and Circulatory Physiology) 292:H3089-H3102.
[30] Clayton RH, Panfilov AV (2008) A guide to modelling cardiac electrical activity in anatomically detailed ventricles. Progress in Biophysics & Molecular Biology 96:19-43.
[31] Nielsen PM, Le Grice IJ, Smaill BH, et al. (1991) Mathematical model of geometry and fibrous structure of the heart. American Journal of Physiology (Heart and Circulatory Physiology) 260:H1365-H1378.
[32] Panfilov AV, Keldermann RH, Nash MP (2007) Drift and breakup of spiral waves in reaction-diffusion-mechanics systems. Proceedings of the National Academy of Sciences 104:7922-7926.
[33] Kohl P, Sachs F (2001) Mechano-electric feedback in cardiac cells. Philosophical Transactions of the Royal Society A 359:1173-1185.

Table 1 Propagating extrasystoles produced in 1-D simulations for each parameter set with EAD duration fixed to 400 ms. A denotes an antegrade extrasystole, and R denotes a retrograde extrasystole.

Period (ms)	Amplitude	Size (mm)		
		5	15	25
20	0.2	0	0	0
40		0	0	0
60		0	0	0
80		0	0	0
100		0	A	A
20	0.4	AR	AR	AR
40		AAR	ARR	AR
60		AAR	AR	AR
80		A	AAR	AAR
100		AR	AR	AR
20	0.6	0	0	0
40		AAR	AARR	AARR
60		AAR	AARR	AARR
80		AARR	AARR	AARR
100		AR	AR	AR

Table 2 Influence of EAD duration on propagating extrasystoles produced in 1-D simulations for each parameter set. A denotes an antegrade extrasystole, and R denotes a retrograde extrasystole. In these simulations EAD amplitude was fixed at 0.4, and EAD region size was fixed at 15 mm.

Period (ms)	Duration (ms)					
	100	200	300	400	500	600
40	0	AR	AR	ARR	AARR	AARR
60	0	AR	AR	AR	AARR	AARR
80	0	AR	AR	AAR	AARR	AARR

Table 3. Number of extrasystoles produced in 2-D simulations for each parameter set. **B** denotes an incomplete cycle of re-entry that was blocked in the EAD capable region, and **R** denotes re-entry through the EAD capable region that was sustained for 2 or more cycles. In these simulations EAD amplitude was fixed at 0.4.

Period (ms)	Duration (ms)	Radius of EAD capable region (mm) 10	20	25
40	200	1	1	1
60		1	1	1
80		1	1	1 **B**
100		1	1	1
40	400	2	2	2
60		2	2 **R**	1 **R**
80		2 **B**	2 **B**	1 **B**
100		1	1	1
40	600	3 **B**	2	3 **R**
60		3 **B**	3 **R**	3 **R**
80		2	2	2
100		2	2	2

Figure captions

Figure 1. Action potentials in the 4VSIM model for normal regions (a), and EAD capable regions (b). Inset in (a) shows action potential duration restitution curve.

Figure 2. Explanation of space-time plots used in Figures 3 and 4 to show behaviour of 1-D fibres. The 40 mm long fibre was stimulated at the beginning of the simulation, and the action potential propagates along the fibre. Panels (a), (b) and (c) show the transmembrane potential 30 mm, 20 mm and 10 mm from the location of the stimulus respectively. The central region shown in (b) is EAD capable, and produces an antegrade action potential shown in (a), and two retrograde action potentials shown in (c). The overall behaviour of the fibre is summarised in the space-time plot shown in panel (d), where the transmembrane voltage is encoded as greyscale, and the transmembrane potential time series shown in (a), (b), and (c) are shown as horizontal lines.

Figure 3. Effect of changing the size of the EAD capable region and the EAD amplitude in 1-D simulations. The top row shows simulations with size of 5 mm, duration 400 ms, period 60 ms, and amplitude of 0.2 (left), 0.4 (middle), and 0.6 (right). The middle and bottom rows show simulations with the same set of parameters except that in the middle row size is 15 mm, and in the bottom row size is 25 mm.

Figure 4. This figure shows the effect of changing EAD duration and EAD period for a 1-D fibre with EAD region size of 15 mm, and EAD amplitude of 0.4. Each row shows space-time plots for duration of 100 ms (left), 200 ms, 300 ms, 400 ms, 500 ms, and 600 ms (right). EAD period is 40 ms (top row), 60 ms (middle row), and 80 ms (bottom row). Duration has a strong influence on the number of propagating extrasystoles, which is only modulated slightly by period

Figure 5. Snapshots of EAD behaviour in 2-D simulation with EAD radius 20 mm and EAD duration 400 ms, period (a) 40, (b) 60, (c) 80, and (d) 100 ms. Each snapshot shows transmembrane potential in 6 x 6 cm tissue sheet, encoded using the same scheme as Figures 2-4. See text for other details. Movies of these simulations are provided as supplementary data.

Figure 1

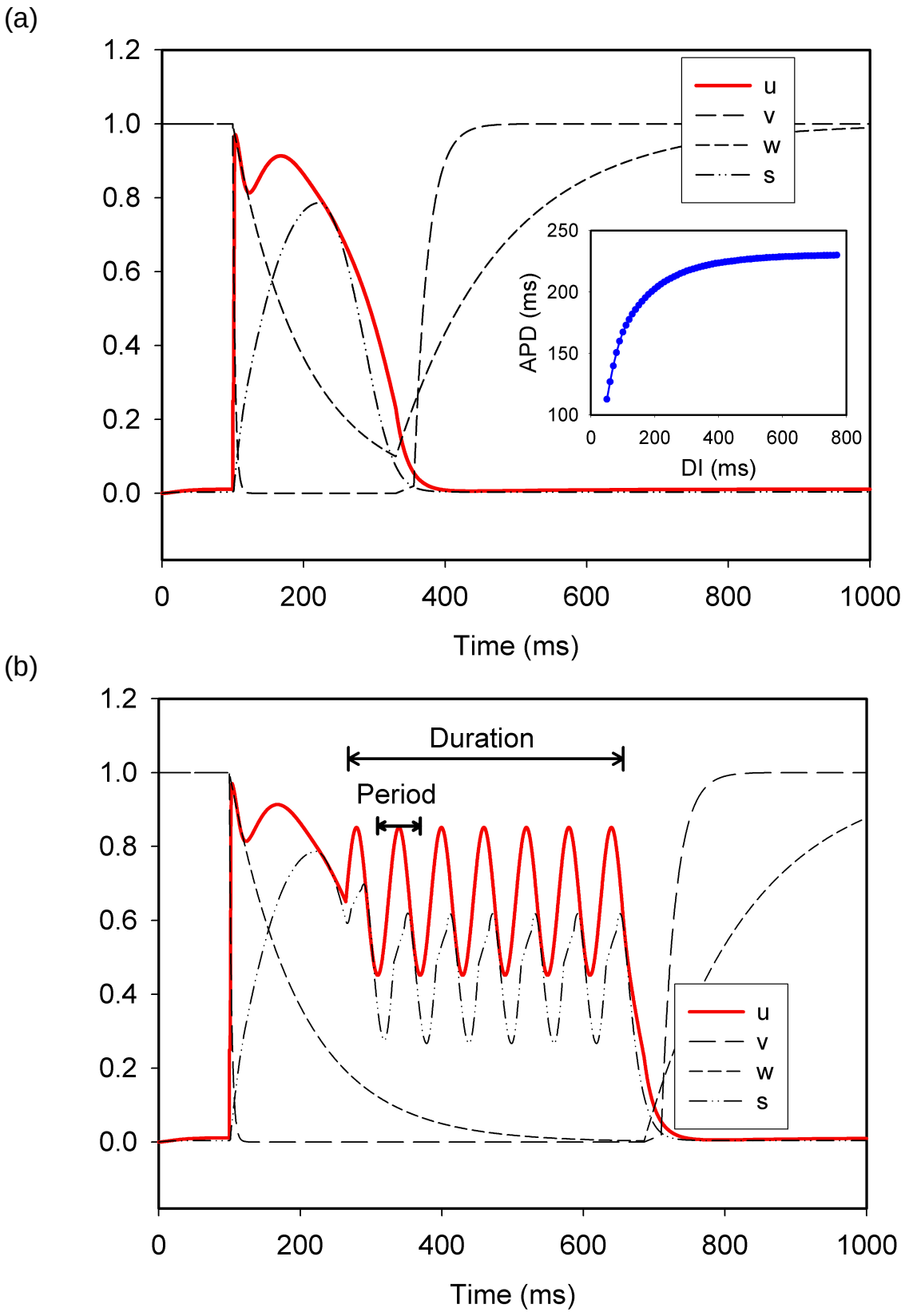
(a)
1.2
1.0
0.8
0.6
0.4
0.2
0.0
0
200
400
600
800
1000
Time (ms)
u
v
w
s
APD (ms)
250
200
150
100
0
200
400
600
800
DI (ms)
(b)
Duration
Period
1.2
1.0
0.8
0.6
0.4
0.2
0.0
0
200
400
600
800
1000
Time (ms)
u
v
w
s

Figure 2

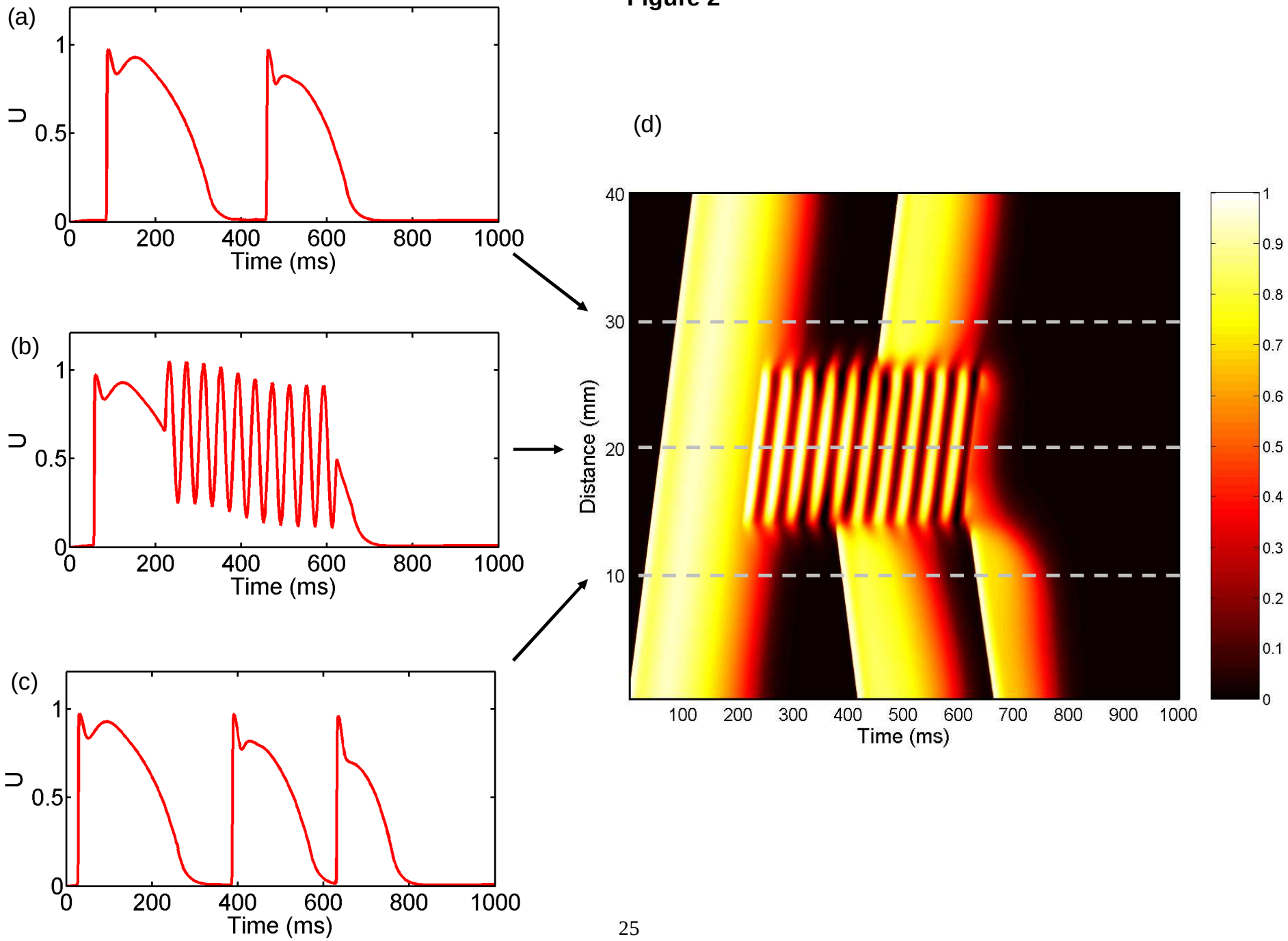

Figure 3

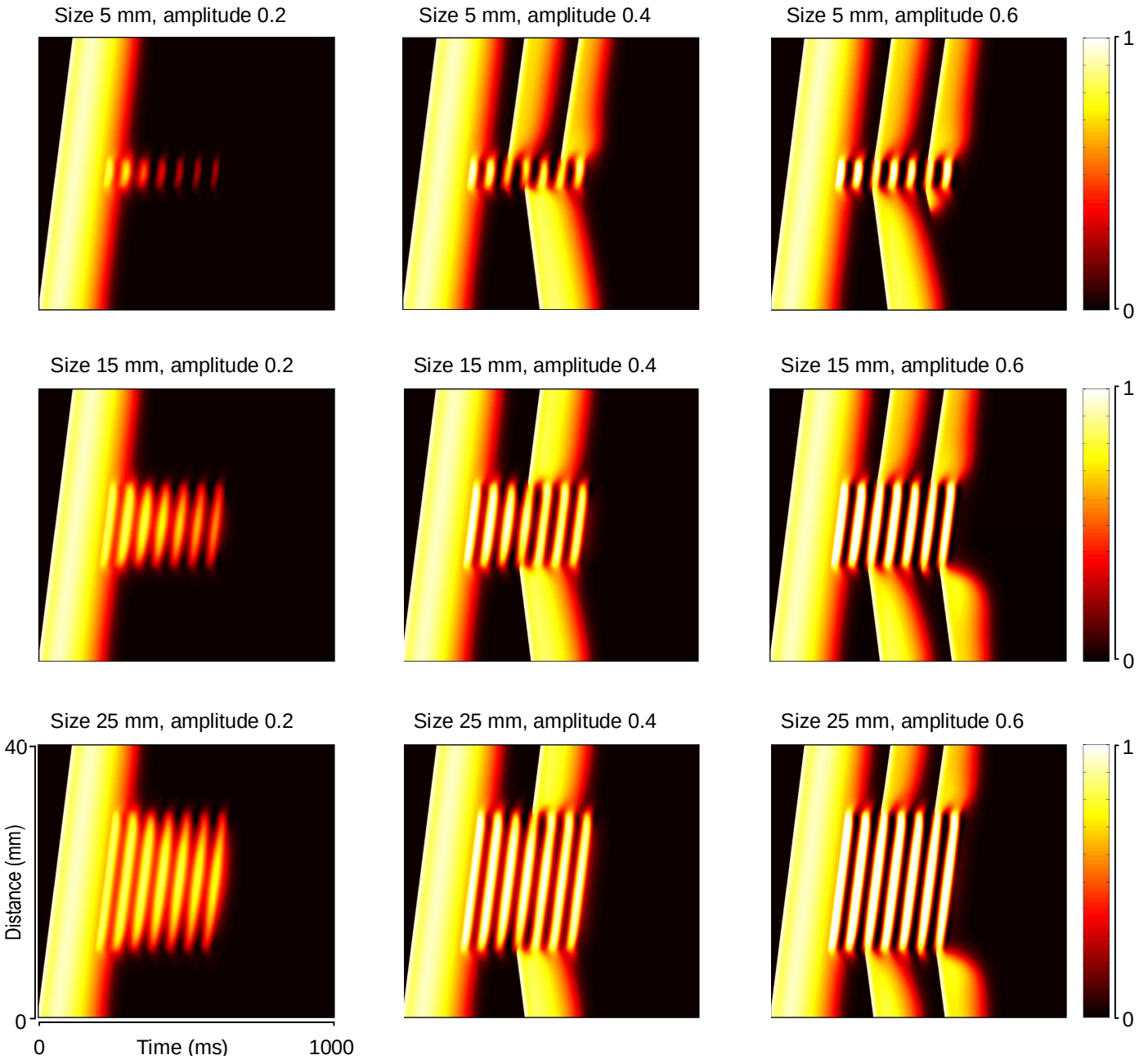
Size 5 mm, amplitude 0.2
Size 5 mm, amplitude 0.4
Size 5 mm, amplitude 0.6
1
0
Size 15 mm, amplitude 0.2
Size 15 mm, amplitude 0.4
Size 15 mm, amplitude 0.6
1
0
Size 25 mm, amplitude 0.2
Size 25 mm, amplitude 0.4
Size 25 mm, amplitude 0.6
40
Distance (mm)
0
0
Time (ms)
1000
1
0

Figure 4

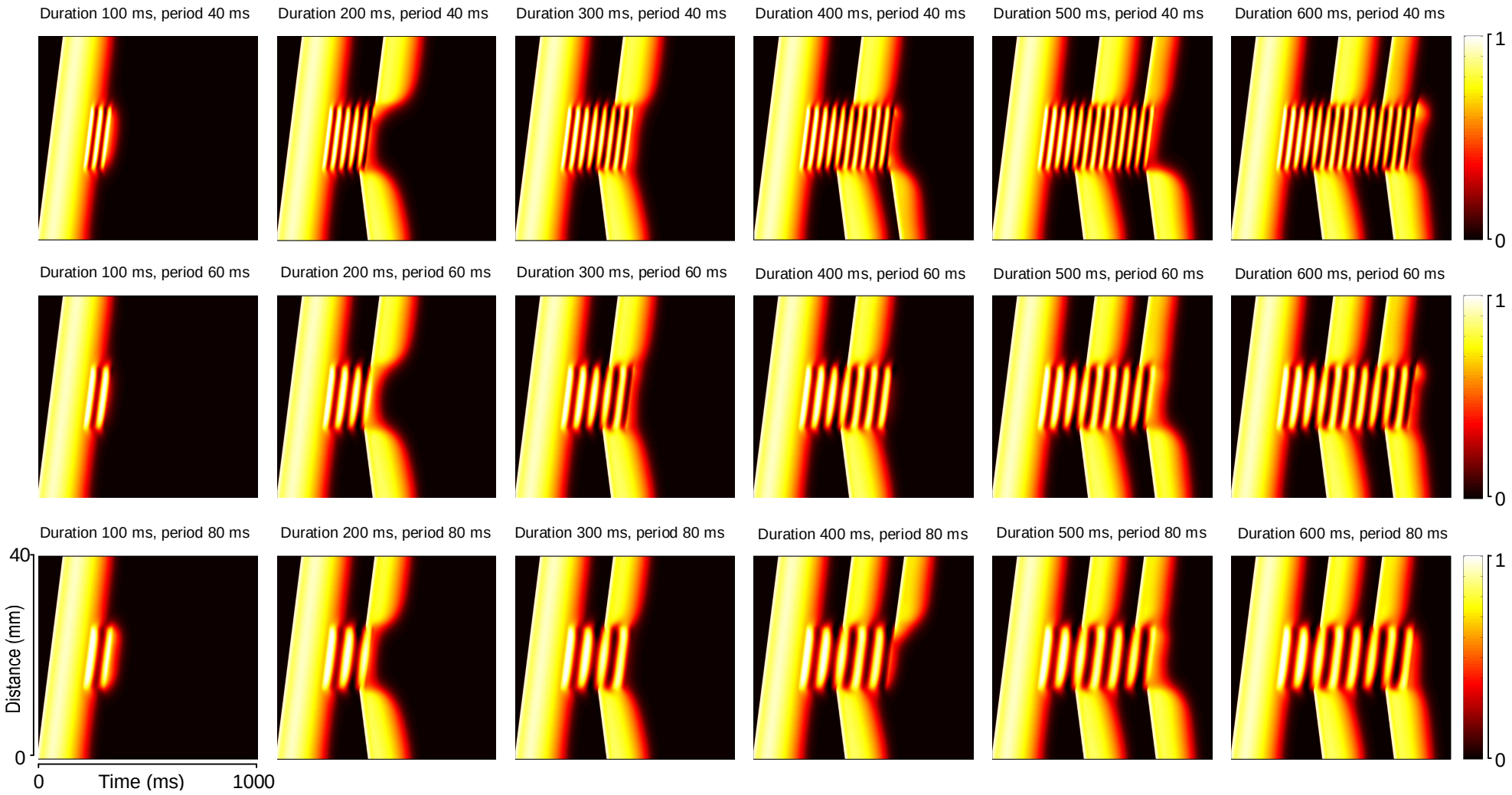
Duration 100 ms, period 40 ms
Duration 200 ms, period 40 ms
Duration 300 ms, period 40 ms
Duration 400 ms, period 40 ms
Duration 500 ms, period 40 ms
Duration 600 ms, period 40 ms
Duration 100 ms, period 60 ms
Duration 200 ms, period 60 ms
Duration 300 ms, period 60 ms
Duration 400 ms, period 60 ms
Duration 500 ms, period 60 ms
Duration 600 ms, period 60 ms
Duration 100 ms, period 80 ms
Duration 200 ms, period 80 ms
Duration 300 ms, period 80 ms
Duration 400 ms, period 80 ms
Duration 500 ms, period 80 ms
Duration 600 ms, period 80 ms
1
0
1
0
1
0
40
Distance (mm)
0
0
Time (ms)
1000

Figure 5